JOURNAL OF ENGINEERING SCIENCES

Volume 10, Issue 2 (2023)

Livatyali H. (2023). A novel force control strategy for improved surface integrity in low plasticity burnishing. Journal of Engineering Sciences (Ukraine), Vol. 10(2), pp. A18–A26, doi: 10.21272/jes.2023.10(2).a3

A Novel Force Control Strategy for Improved Surface Integrity in Low Plasticity Burnishing

Livatyali H.[0000-0002-9542-2390]

Mechatronics Engineering Department, Yildiz Technical University, Barbaros Blvd., Besiktas, 34349 Yildiz-Istanbul, Turkey

Article info:

Submitted:	July 12, 2023
Received in revised form:	September 14, 2023
Accepted for publication:	September 25, 2023
Available online:	September 26, 2023

***Corresponding email:**
hlivatya@yildiz.edu.tr

Abstract. Ball burnishing is a cold work process where a hard ceramic or diamond ball rolls on a metal surface and flattens the roughness peaks under high local pressure. The small deformation created on the surface imposes compressive residual stresses and raises hardness in a shallow sub-surface layer, leading to improved fatigue, corrosion, and foreign object damage performances. Trial-and-error type experimental work to determine the optimum process parameters for a cold-forming process like ball burnishing for acceptable performance is costly. Therefore, the article aims to investigate the effects of various force control strategies in the double-sided low plasticity burnishing (LPB) process to find the effects on deformation and residual stresses on thin Ti_6Al_4V flat sheets. A 3D static-implicit finite element model was developed with an elastic-rigid plastic flow curve. Simulations were conducted to predict residual stresses and deformationi on the surface. As a result, it was proven that ball burnishing can produce a deterministically controlled surface. An increased vertical force produced higher deformation normal to the surface and, therefore, a deeper pool. As the ball proceeded further, a plowing effect developed such that when a 3.5–4.8 μm deep pool was formed (at a vertical force of 150 N), a peak of 2.8 μm was produced at the front end. Overall, the deformation on the surface and the residual stresses were directly interrelated. Parallel to the deformation on the surface, residual stresses on and beneath the surface also showed some variation. Nevertheless, the predicted residual stress variations were not big. They did not switch to the tensile mode in the burnished zone. Therefore, the whole sheet surface should be burnished to obtain all the compressive residual stresses.

Keywords: ball burnishing, residual stress, finite element analysis, process innovation.

1 Introduction

Finishing processes determine the surface quality of mechanical components because of the direct effects on their performance and service life. The surface integrity of an engineered surface is generally characterized in terms of surface finish, micro-hardness, and the state of residual stress. These properties control functional surfaces' fatigue, corrosion, wear, and foreign object damage performances under mechanical loading.

In general, fine surface finish, high hardness, and compressive residual stresses are required for good performance [1, 2]. Therefore, the final surface finishing operation directly influences the functionality of the components under service conditions.

The burnishing process usually follows a finish turning or milling operation, and it is seen as an alternative to abrasive processes (e.g., grinding, polishing) or a surface forming process such as shot peening [3].

Regardless of the manufacturing method, all surfaces have a series of peaks and valleys at variable heights. In the burnishing process, to deform the surface layer and flatten these peaks, a smooth free-rolling spherical ball or axisymmetric roller is employed at a single pass or several passes (up to 7–8) under limited normal force (Figure 1) [4].

The ball or roller is rolled (as an idler) across the surface of the workpiece, applying vertical force on the surface such that elastic-plastic deformation takes place on the surface layer. Consequently, a strain-hardened, smoother surface with compressive residual stress on the surface layer and towards the depth of the material is introduced.

Burnishing can be applied on a dedicated machine tool, a CNC lathe on an axisymmetric part, or a vertical milling machine on a flat part or a part with a more complex 3D surface. It is primarily a cold-forming process but rarely applied under hot or warm forming conditions.

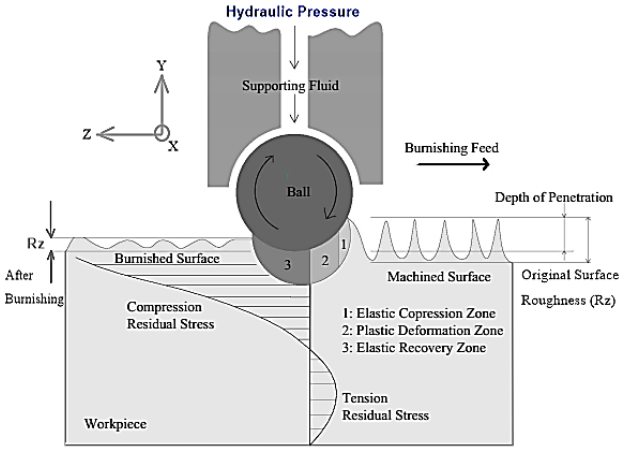

Figure 1 – Schematic representation of ball burnishing of a flat surface

It is mostly a displacement-controlled process, but some force-controlled applications also exist. Tool material may be high carbon alloy steel, tungsten carbide, silicon nitride, or diamond, while the workpiece material ranges from many casts to wrought alloys and, recently, additively manufactured metals. It has two common types of applications in terms of the amount of plastic deformation: low-plasticity burnishing (LPB) [1] and deep rolling (high plasticity). The difference is that the latter is usually applied in a relatively shallow single pass, while deep rolling involves more significant plastic strains applied in two, three, or more passes.

Roller burnishing is limited to the processing of axisymmetric parts because the forming roller has a fixed axis of rotation, and it is used like a cylindrical turning or facing tool. On the other hand, ball burnishing can be employed on a lathe to process axisymmetric parts and on a milling machine to burnish flat or 3D surfaces [5]. The ball burnishing tool holders used for axisymmetric parts are geometrically very similar to lathe tools (with a large negative rake angle), and both LPB and severe rolling may be applied with them. The ball burnishing tools designed for milling machines look like ball end mills, and the carbide or ceramic ball is hydraulically supported to minimize friction and facilitate heat removal.

2 Literature Review

Kalmegh and Klocke's review paper [6] is on enhancing the mechanical properties of metal alloys via LPB. This review gives a good comparison of LPB and conventional ball and roller burnishing.

Accordingly, most academic research on burnishing focuses on improving surface roughness and hardness. However, the potential of generating compressive residual stresses and, thus, improvement of fatigue, corrosion, and wear performances are not covered. They reported that LPB produced better results in terms of corrosion and high-temperature behaviors for most metals.

Burnishing may be applied under dry, flooded, MQL (minimum quantity lubrication), cryogenic, or hybrid (MQL at cryogenic temperature) lubrication and cooling modes [7].

Lubrication in burnishing is critical to control friction at a sustainably low level and to remove the heat generated by friction and plastic deformation. Dry lubrication is an extreme case and is not feasible in mass production. The industrially standard flooded lubrication uses water-based emulsions such as boron oil. The lubricant is also used as the hydraulic support (bearing) fluid in LPB. As alternatives to promote sustainable manufacturing, MQL (minimum quantity lubrication), cryogenic lubrication using liquid Nitrogen (LN_2), and hybrid lubrication combining these two modes are proposed [7]. While MQL does not produce attractive results, cryogenic and hybrid lubrication modes are very effective without much difference. LN_2 functions both as a coolant that enables a cold deformation with dynamic recrystallization on the part surface and a lubricant that keeps friction at a low level to minimize power consumption of the process and minimize tool wear.

Regarding metal type, there is no limitation of hardness or strength; however, ductile alloys are easier to process, while relatively brittle metals require additional effects such as ultrasonic or higher amplitude vibrations or some pre-heating [8].

Caudill et al. [9] demonstrate the effects of roller burnishing as applied in the form of deep rolling on the surface topology of cylindrical parts (of Ti_6Al_4V). They compared the surface roughness obtained using flooded, MQL, cryogenic, and hybrid (MQL + cryogenic) modes in terms of the number of burnishing passes. Overall, hybrid cooling gave the least average surface roughness at four passes.

Caudill et al. [10] also showed surface hardness as a function of burnishing feed at two vertical force levels under flooded, MQL, cryogenic, and hybrid cooling conditions. Accordingly, cryogenic and hybrid cooling modes gave the highest surface hardness, feed, and vertical force, not showing a significant effect. Cooling mechanisms substantially affect hardening, and hybrid cooling has a more consistent effect than cryogenic cooling, which cannot always penetrate sufficiently fast.

A similar situation is reported by Huang et al. [11] on AA 7050-T7451. The notable effect of cryogenic cooling is dominant on the surface, and it diminishes along the depth from the surface because of the refined and transition layers formed by cryogenic cooling.

Travieso-Rodríguez et al. [12] worked on the hardening effect and fatigue behavior enhancement of ball burnishing on cylindrical AISI 1038 steel parts. Their fatigue tests and hardness measurements revealed that ball burnishing increases the expected fatigue lifespan for the specimens through cold work and strain hardening.

The other effect of burnishing is crystallographic texturing on the surface layer. The cold deformation generates dominant basal textures like cold rolling [13].

Burnishing usually causes severe grain refinement. The sub-surface nano-grains produced during the hybrid burnishing of Ti_6Al_4V cylinders occurred at depths up to 1 micron beneath the finished surface [9]. Grain sizes were

measured in the range of 54–212 nm, which indicates dislocation motion and grain boundary strengthening in this layer. A more severe grain refinement may also cause softening, as shown in Co-Cr-Mo alloy [14].

One paper that demonstrates the effect on residual stress after two-sided LPB of a cold rolled Ti_6Al_4V sheet was published by Livatyali et al. [15]. Closed square areas were burnished, and the variation of residual stresses on the surface and underlayer were shown. Accordingly, compressive residual stresses are formed inside the burnished surface, and this phenomenon can be predicted more accurately using a 3D static-implicit model. The residual stress on the surface is consistently compressive independent of vertical force, but under the surface, the compressive stress increases for a while, and it may switch to tensile as it gets deeper. Compressive residual stresses are needed on the surface, and burnishing can provide that, and the balancing tensile residual stress at the neutral plane would not deteriorate the fatigue or corrosion performance of the component. Ball burnishing is an interesting surface cold-forming process such that the processed area is covered deterministically by controlling either the force or displacement (penetration). Consequently, compressive residual stresses in both planar directions induce the burnished pool surface.

Pu et al. compared improvements in corrosion behavior in the ground, dry, and cryogenic roller-burnished AZ31B samples [13]. There are significant differences in corrosion morphology between the samples processed by grinding and cryogenic burnishing, while the differences between burnished samples under dry and cryogenic conditions are significantly smaller. The ground surface after immersion is rough, with large and deep pits all over the surface. There are only some small pits on both burnished surfaces, and the corroded areas of the burnished samples are smaller than the ground ones. These suggest that much less Mg was corroded from the burnished surfaces than the ground surface.

The technical problem elaborated in this article is inspired by the previous results [16]. When the hydraulic (support) pressure in the LPB tool is kept constant (such as at 50, 100, or 150 bar), the burnished pool depth does not come out as a perfectly flat surface such that there is some depth variation along the feed (longitudinal) and traverse (lateral) directions. Residual stress distribution also has variations. Besides, the predominantly positive residual stress may switch to positive by the edges of the burnished pool. A relatively homogeneous residual stress distribution is required to avoid unexpected performance variation. Therefore, this study aims to improve the flatness and homogenize the compressive residual stresses of the burnished surface by controlling or adjusting the hydraulic pressure. A previously validated finite element model was used in simulations to prove the hypothesis, and the results were evaluated and discussed.

3 Research Methodology

3.1 Material

Due to its versatility, ASTM Grade 5 titanium (Ti6Al4V) is the most used titanium alloy. The chemical composition of this alloy is outlined as 87.6–91.0 % Ti, 5.50–6.75 % Al, 3.5–4.5 % V, less than 0.40% Fe, and O, C, N, and H in relatively small proportions.

It is an alpha-beta titanium alloy with aluminum stabilizing the alpha phase and vanadium stabilizing the beta phase. The hardness of the annealed stock is typically 300 BHN. After aging at 524–552 °C, typical hardness reaches 360 BHN. Ti_6Al_4V is widely used because of its optimum blend of properties (Table 1) [17].

Table 1 – Material properties of Ti_6Al_4V (cold rolled, precipitation hardened)

Property	Unit	Value
Elasticity modulus	GPa	114
Poisson's ratio	–	0.31
Yield strength	MPa	1100
Tensile strength	MPa	1170
Maximum elongation	%	10
Density	kg/m^3	4430

It can undergo further processing to suit better to specific requirements.

Ti_6Al_4V is neither a strain hardening nor a ductile material with a maximum elongation of 10 %. The slight difference between the yield and tensile strengths shows that it strain-hardens slightly. LPB is a locally applied compressive process. Therefore, the tensile elastic-plastic flow curve is not representative, but no better data is available. Therefore, tensile data is used in the finite element model. The flow curve was modeled as a piece-wise linear curve since the traditional power law does not accurately model this alloy's flow behavior.

3.2 Modeling

Deformation in ball burnishing of flat parts is a complex 3D process. Simulation of metal forming operations using 3D finite element models gradually increased in the 1990s. However, it is not always practically useful due to hardware and time limitations in the industry. A 2D model offers practical and valuable results in burnishing axisymmetric parts by turning [18, 19]. However, the plane-strain constraint for the 2D model prohibits the materials from flowing along the out-of-plane direction, whereas in the 3D condition, the surface materials flow in all directions.

In the model, temperature rise due to plastic deformation was neglected because the fluid in the system also serves as a coolant. The ball's movement can be controlled in two ways in the finite element analysis: force and displacement control. The static-implicit force control method comes with limited control and convergence problems. Thus, the displacement control method was used in the simulations. The $p = F/A$ formula was used with 90 % effectiveness in obtaining appropriate force values to predict the experimental force.

The ball was modeled as a rigid body based on studies indicating the modeling ball as an elastic body, only increasing the computer running time. The commercially available non-linear finite element program, ANSYS® v.10, was employed to simulate the burnishing process. In the experimental study, the two-sided burnishing tool constituted a symmetry condition; half of the workpiece geometry was meshed.

Small-time steps and indentation depths are known to improve accuracy and time. In the 3D model, several different time steps were applied, with a measure of 0.0005 s/step finally selected (Table 2).

Table 2 – Process parameters used in the industrial tests and FE simulations

Property	Unit	Value
Sheet thickness	mm	1.270
Sheet length	mm	3.302
Sheet width (3D model)	mm	3.302
Ball radius	mm	6.350
Ball material	–	Tungsten Carbide
Ball pressure	bar	50, 100, and 150
Tool speed (longitudinal)	mm/s	1.5240
Traverse feed	mm	0.0762
Number of passes	–	20
Time step	S	0.0005
Simulated burnish $L \times W$	mm	1.524×1.524

The finite element model with 8092 8-node elements with 0.1 mm edge length (Solid 45) was then prepared. Solid45 is also a hybrid type element that can simulate elastic-plastic metal flow. The ball diameter came to 6.35 mm, with the dimensions of the workpiece coming to 3.302×3.302×0.635 mm.

The boundary conditions of the finite element models are the primary inputs affecting the results verified once again during ball burnishing simulations [20]. The displacement constraints that were applied on the left, right, and bottom boundaries of the workpiece are shown in Figure 2.

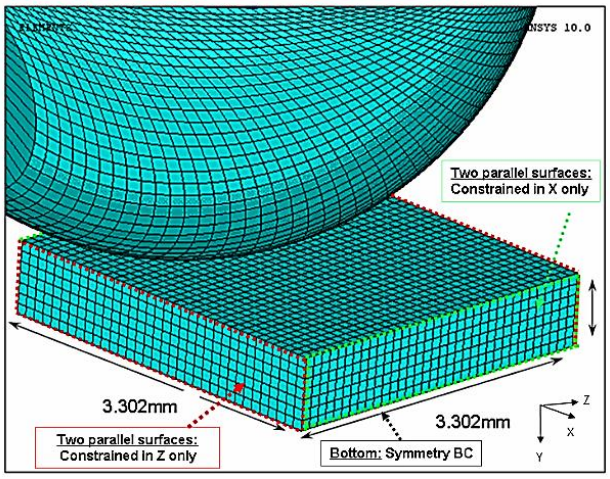

Figure 2 – 3D mesh and the boundary conditions

The ball changes the direction of motion four times to complete one burnishing pass in the simulations. Each pass was run at a tool speed of 1.524 mm/s.

0.0005 s was selected as a time step, giving stable conversion after many iterations. The ball was lifted from the surface and moved horizontally according to a distance equal to the traverse feed of 0.0762 mm at the end of each pass. A total of 20 burnishing passes were performed (Figure 3).

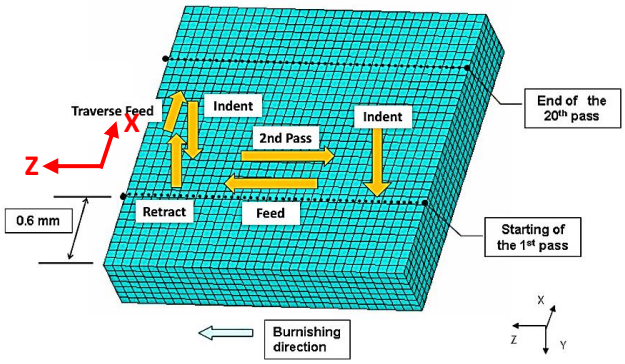

Figure 3 – Passes in the 3D FE simulation of LPB

The standard contact model in ANSYS was sufficiently consistent and used. Previously, the tested DEFORM 3D contact model did not give the precise surface behavior needed in burnishing.

Experimental data used to validate the results of simulations were obtained from the General Electric Aircraft Engines Co. [15]. An LPB process was conducted with a tool that can apply double-sided polishing to a Ti_6Al_4V sheet of 1.27 mm thickness to represent typical turbine blades (Figure 4) [21].

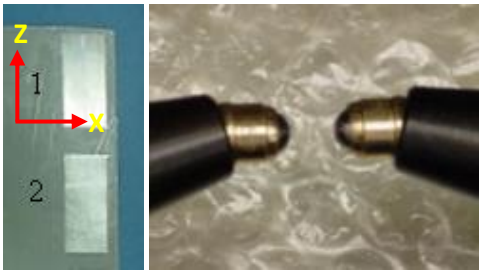

Figure 4 – Ti_6Al_4V sheet specimen and double-sided LPB tooling (provided by GEMTC)

Experiments were conducted at 50, 100, and 150 bar ball burnishing pressures. The experimental residual stress results were obtained over the surface and depth of the material in axial (parallel) and lateral (perpendicular) directions. The X-ray diffraction method was used to measure the residual stresses. Since the validation phase was published earlier [15], process design and enhancement are the focus of the current article.

As expressed earlier, boundary conditions are essential in predicting any elastic-plastic deformation and, thus, those in ball burnishing simulations. An additional simulation was performed as a model verification attempt such that a four times larger workpiece was meshed, the

burnished square pool was four times more significant, and 100 bar was taken as the pressure [15]. The predictions were not significantly closer to the experimental results; therefore, the 3.4×3.4 mm model was used for further process optimization, as presented in this paper.

4 Results

4.1 Deformation in LPB and residual stresses

Figure 5 shows the permanent vertical displacement after a 20-pass LPB simulation at 50 bar pressure. Accordingly, the maximum downward permanent movement was predicted as 1.63 µm. The exact figure is also used to demonstrate the mid-section cuts made to visualize the profile surfaces in X (lateral) and Z (longitudinal) directions.

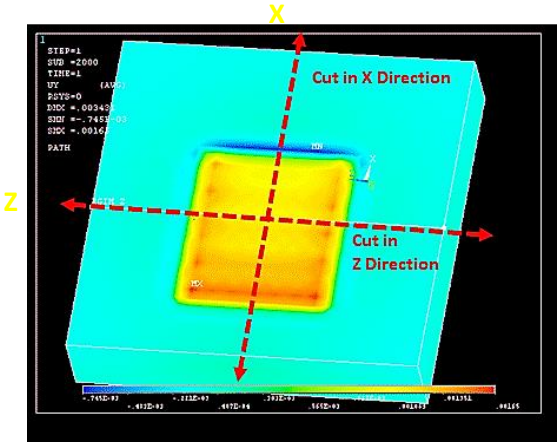

Figure 5 – Vertical displacement distribution after a 20-pass LPB simulation at 50 bar hydraulic pressure

LPB is a single-pass burnishing process applied with relatively low plastic deformation. When the ball moves forward parallel to the surface along the feed direction, the material is displaced sideways in the traverse (lateral) direction. As the ball is shifted in the amount of predetermined traverse feed and fed in the reverse direction for the second pass, the lateral material movement occurs in a single direction towards the not-yet-burnished one. The effect of this displacement is that the pool generated by the burnishing passes gets gradually shallower in the lateral direction until it converges to a fixed value. This phenomenon can be visualized in Figure 6 such that an inward shift of 0.4 µm is predicted where the deepest point is about 1.5 µm.

On the other hand, the back-and-forth movement of the ball in the feed (Z) direction generates an approximately symmetrical shape, as depicted in Figure 7. Besides, the plowing effect on both sides is less than 0.05 µm, while it is again 0.05 µm at the edge of the initial pass and 2.0 µm at the 20th and final pass (Figure 6).

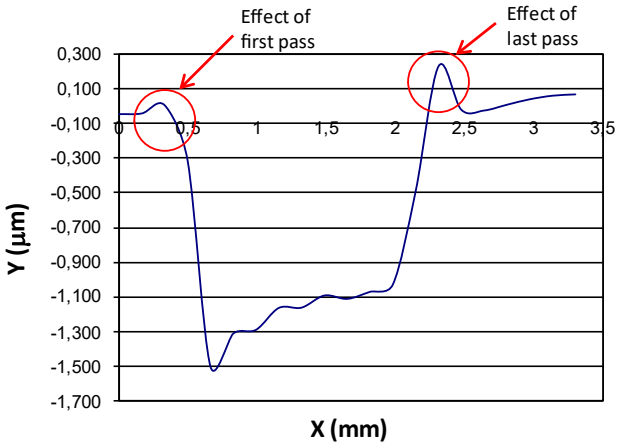

Figure 6 – Surface profile predicted at the mid-section of the workpiece along the X (lateral) axis

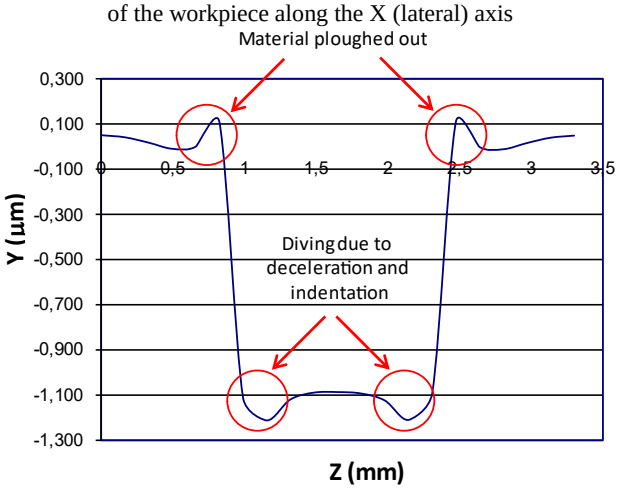

Figure 7 – Surface profile predicted at the mid-section of the workpiece along the Z (feed) axis

As explained above, a rolling ball in the longitudinal direction plows and displaces the metal in the lateral direction, forming the burr at the edge. To get rid of this burr, the burnished passes should be continued until the ball gets out of the metal plate and the burr is flattened out.

Since the process is elastoplastic, the solid material displacement ends with a residual stress distribution. Fortunately, the residual stresses generated by ball burnishing are compressive on the surface; however, as seen in the sideways plowing effect, a narrow band of small positive residual stress may be generated at the pool edges.

Figure 8 shows the lateral (X) residual stresses after LPB at 50 bar and the cross-sections on which the deformation is analyzed.

From this figure, the planar residual stress in the X direction is relatively low along the axis of the first pass, and it reaches the highest magnitude by the 20th pass. The phenomenon is discussed along the numbered axes for a clearer understanding of surface deformation and the planar residual stresses.

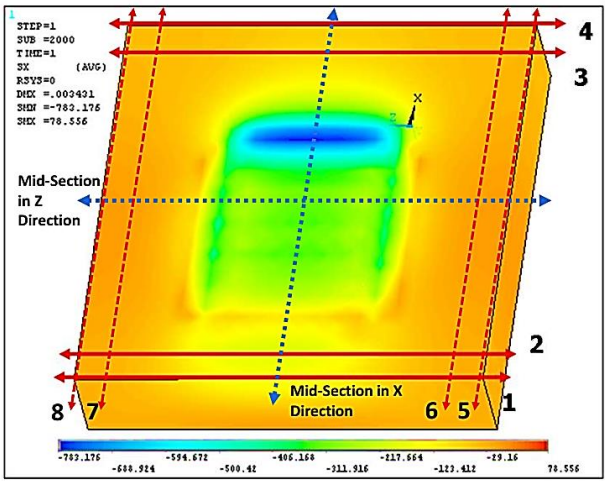

Figure 8 – X-residual stress distribution after LPB at 50 bar and the cross-sections of the deformation are analyzed

Figures 9 and 10 show the predicted residual stresses in the X and Z axes along lateral (X, left) and feed (Z, right) directions after LPB at 50 bar along the sections near the edges (1 through 8, as shown in Figure 8).

The results show that the value of the compressive state of stress diminishes towards the edges. The exciting aspect is that the variation of Z-residual stress along the X direction and the variation of X-residual stress along the Z direction are very similar (Figure 9). The same trend is visible in Figure 10 as well.

When the X component of residual stress becomes more compressive, the Z component gets less compressive, keeping the mean planar stress almost constant on the compressive side. The deviations from symmetry in Figure 10 reflect the plowing effect and burr formation on the leading edge discussed above.

From here, it may be concluded that the residual stresses are independent of direction (either feed or lateral) out of the burnished pool. Besides, the compressive nature of the residual stresses does not change with a gradual fading effect.

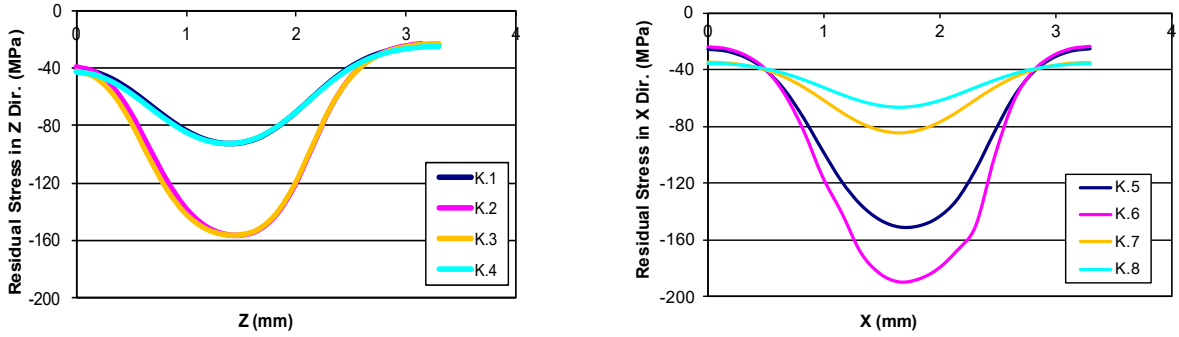

Figure 9 – Residual stresses in the X-axis predicted after LPB at 50 bar along X lateral (a) and Z feed (b) directions

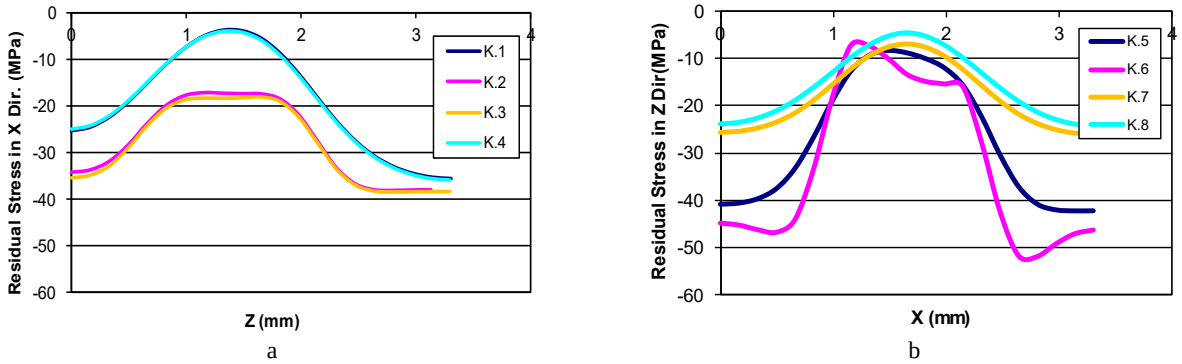

Figure 10 – Residual stresses in the Z-axis predicted after LPB at 50 bar along X lateral (a) and Z feed (b) directions

4.2 Optimizing the surface profile and residual stress distribution

As discussed above and in the previous publication [15], the pool formed by burnishing at constant pressure, which is the force control method used in LPB using the hydraulically supported spherical tool, does not have the leading edge forms a flat base, and a burr with a significant height as the hydraulic pressure gets more significant.

Such behavior is depicted in Figures 11 and 12 on the surface profiles after LPB at 50, 100, and 150 bar, along the Z and X axis, respectively.

The three profiles are symmetric along the feed (Z) axis. However, due to the plowing effect, the burr on the left side of the first pass (trailing side) is much smaller than the one on the right side of the 20th and last (leading) pass.

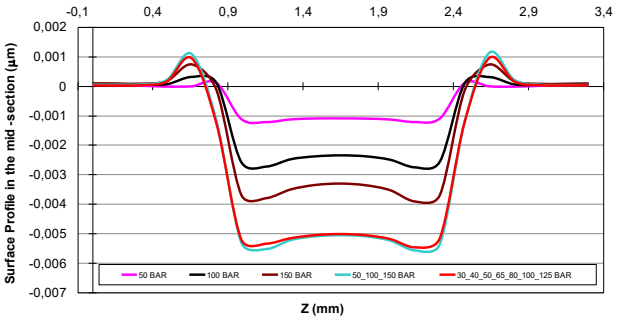

Figure 11 – Surface profiles predicted at the mid-section of the workpiece along the Z (feed) axis at various pressure modes

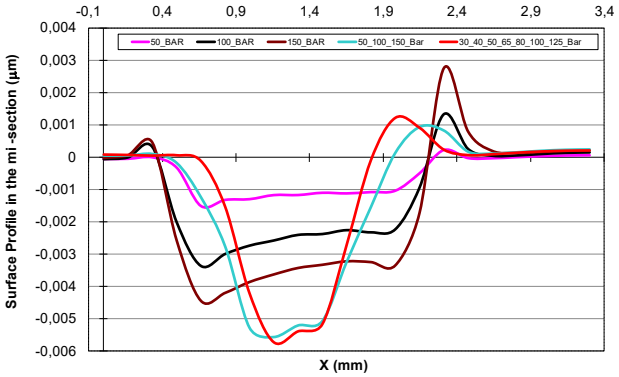

Figure 12 – Surface profiles predicted at the mid-section of the workpiece along the X (lateral) axis at various pressure modes

An attempt has been made to overcome the leading-edge burr problem by applying a variable hydraulic pressure on the spherical tool. In addition to the three initial fixed pressure settings, gradually increasing schemes, including 50–100–150 and 30–40–50–65–80–100–125 bar in subsequent passes, are tested via finite element modeling to see their effects on the surface. Effects of the gradually increased alternative pressure settings can be compared with fixed pressure (at 50, 100, and 150 bar) during LPB in Figures 11 and 12.

Accordingly, the depth of the surface profiles in the Z-direction is almost identical for the two alternative (gradually increasing) schemes; both are deeper than the three fixed-pressure applications. However, the burrs on both sides are also slightly higher (Figure 11). The patterns of the surface profiles are very similar except for the predicted pool depths.

The surface profiles of different pressure settings along the X (lateral) axis exhibit significantly different surfaces (Figure 12). The gradually increased pressure schemes produced no burr on the trailing edge of the first pass, and they produced less burr (at the leading edge of the 20th and last pass) compared to fixed-pressure settings at 100 and 150 MPa. The gradually increased and decreased pressure settings are predicted to produce more tapered pool surfaces, but they do not eliminate the plowing effect and, thus, the burr. These simulations have proven that the plowing effect cannot be eliminated; hence, there is no escape from burr formation. If burnishing is performed on the whole surface, there will not be a vertical burr, and the burr will be swept out of the edge to become a lateral one.

The residual stress value and distribution on the surface are more critical than the burr and the surface profile variation. Knowing that the planar residual stresses are not independent of the final surface profile, the relations of hydraulic pressure setting and the residual stresses are worth elaboration.

Figure 13 shows variations of Z-residual stresses along the Z (feed)-axis on the mid-section (Figure 8) after LPB at various schemes with controlled hydraulic pressure.

Accordingly, Z-residual stress depends on the highest pressure applied; even if the pressure increases gradually, the highest (compressive) residual stress does not change. The X (lateral) component shows a different trend than the Z component (Figure 14).

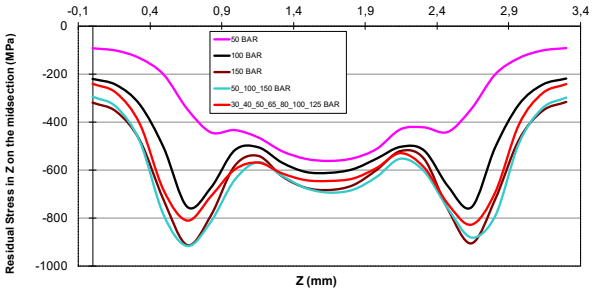

Figure 13 – Variations of Z-residual stresses along the Z (feed)-axis on the mid-section after various processes with controlled hydraulic pressure

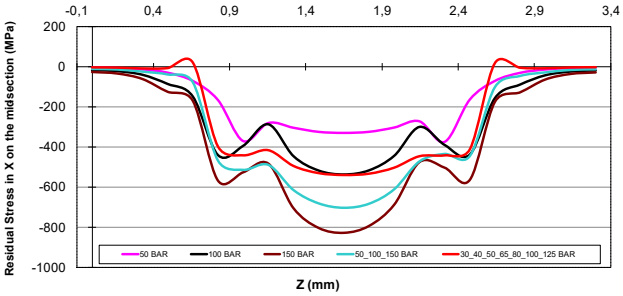

Figure 14 – Variations of X-residual stresses along the Z (feed)-axis on the mid-section after various processes with controlled hydraulic pressure

As the pressure increases, both the compressive stress and its oscillations increase, and gradually increased pressure reduces oscillations of the residual stress rather than the maximum value it reaches. The 30–40–50–65–80–100–125 bar scheme produced an interesting result: narrow zones at the initial and final edges of the pool show a small positive residual stress. From here, it is shown that extremely low burnishing pressure does not help but may even harm the residual stress profile required.

A weaker but similar trend is depicted in Figure 15, in which the Z-residual stress becomes slightly positive along the initial pass when the burnishing pressure is kept smaller.

Figure 16 shows the variation of the X-residual stress along the X (lateral)-axis on the mid-section after various processes with controlled hydraulic pressure.

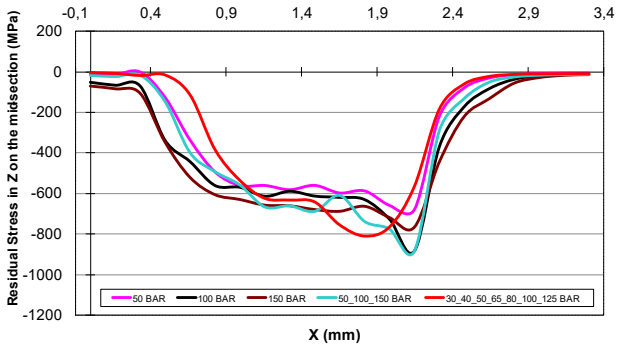

Figure 15 – Variations of Z-residual stresses along the X (lateral)-axis on the mid-section after various processes with controlled hydraulic pressure

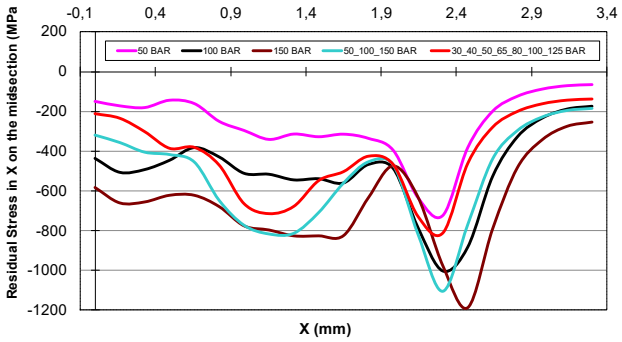

Figure 16 – Variations of X-residual stresses along the X (lateral)-axis on the mid-section after various processes with controlled hydraulic pressure

The magnitude of the compressive residual stress increases as the pressure increases, and the 20th pass obtains the highest value. The gradual increase and decrease of the pressure do not change the trend but just reduce the lowest value the compressive stress (compressive) reaches. This may be seen as a homogenization effect that may be regarded positively but is not strong.

5 Discussions

Overall, neither the surface profiles nor the planar residual stress components are improved remarkably by changing the hydraulic pressure from pass to pass. However, it is seen that as the pressure increases, higher surface deformation, larger burrs, and higher (compressive) residual stresses may be obtained. As an intermediate value, the burnishing simulations at 100 MPa produced moderate deformation and residual stress results that are the most favorable.

Increased hydraulic pressure, that is, vertical force, produces higher deformation normal to the surface and, thus, a deeper pool in LPB. As the ball moves in the feed direction, plowing occurs in the lateral direction such that when a 3.5–4.8 μm deep pool is formed, a burr of 2.8 μm is produced at the front end at 150 bar pressure.

Meanwhile, the surface residual stresses reaching –1000 and –1200 MPa (process at 150 bar) are evaluated as an overprediction. One reason for this and overall predictions is considered the rigid boundary conditions of a relatively small coupon. The other one may be due to the use of 8-node linear brick elements that behave stiffly. Therefore, the presented values should not be taken as absolute predictions but should be seen as a relative measure of evaluation.

Residual stresses are elastic stresses, and compressive stresses at a section must be balanced by tensile stress at another one to attain static equilibrium [16]. Therefore, burnishing should not be applied in a pool but on the whole surface creating small burrs at the edges.

6 Conclusions

Improvement of surface topology and residual stress distribution after low plasticity ball burnishing of Ti_6Al_4V sheets has been investigated. For this purpose, the effects of various force strategies were tested using a previously validated 3D static-implicit finite element model.

Results indicate that varying the hydraulic pressure in subsequent passes does not produce a surface profile closer to a flat one. Using a moderate constant pressure is preferable to keep the burr formation minimal by the burnished pool edges and residual stress distribution in a compressive state.

The plastic deformation on the surface and the residual stress distribution are directly interrelated. Surface deformation and residual stresses on and under the surface show some variation. Fortunately, residual stress variations are not considered significant and are dominantly compressive. However, the compressive residual stress at the leading edge is higher than at the beginning edge. That is due to the plowing effect of the moving ball on the part surface.

Acknowledgment

General Electric Marmara Technology Center (GEMTC) Ltd. is gratefully acknowledged for the possibility of carrying out experimental data. Ms. Ergul Has is also acknowledged for the possibility of conducting simulations.

References

1. Prevey, P. S., Shepard, M. J., Smith, P.R. (2001). The effect of low plasticity burnishing (LPB) on the HCF performance and FOD resistance of Ti-6Al-4V. *In: 6th National Turbine Engine High Cycle Fatigue Conf. March 5-8, 2001, Jacksonville, FL, USA*, pp. 1–10. Available online: https://apps.dtic.mil/sti/tr/pdf/ADA447005.pdf
2. Avilés, R., Albizuri, J., Rodríguez, A., López de Lacalle, L. N. (2013). Influence of low-plasticity ball burnishing on the high-cycle fatigue strength of medium carbon AISI 1045 steel. *International Journal of Fatigue*, Vol. 55, pp. 230–244. https://doi.org/10.1016/j.ijfatigue.2013.06.024
3. Shaw, L. L., Tian, J.-W., Ortiz, A. L., Dai, K., Villegas, J. C., Liaw, P. K., Ren, R., Klarstrom, D. L. (2010). A direct comparison in the fatigue resistance enhanced by surface severe plastic deformation and shot peening in a C-2000 superalloy. *Materials Science and Engineering: A*, Vol. 527(4–5), pp. 986–994. https://doi.org/10.1016/j.msea.2009.10.028
4. Luca, L., Neagu-Ventzel, S., Marinescu, I. (2005). Effects of working parameters on surface finish in ball-burnishing of hardened steels. *Precision Engineering*, Vol. 29(2), pp. 253–256. https://doi.org/10.1016/j.precisioneng.2004.02.002
5. Travieso-Rodríguez, J. A., Dessein, G., González-Rojas, H. A. (2011). Improving the surface finish of concave and convex surfaces using a ball burnishing process. *Materials and Manufacturing Processes*, Vol. 26(12), pp. 1494–1502. https://doi.org/10.1080/10426914.2010.544819
6. Kalmegh, A. P., Khodke, P. M. (2017). Review on low plasticity burnishing process: A potential for improving mechanical properties of material. *International Journal of Mechanical Engineering and Technology*, Vol. 8(5), pp. 791–810. Available online: https://iaeme.com/MasterAdmin/Journal_uploads/IJMET/VOLUME_8_ISSUE_5/IJMET_08_05_087.pdf
7. Caudill, J., Huang, B., Arvin, C., Schoop, J., Meyer, K., Jawahir, I. S. (2014). Enhancing the surface integrity of Ti-6Al-4V alloy through cryogenic burnishing. *Procedia CIRP*, Vol. 13, pp. 243–248. https://doi.org/10.1016/j.procir.2014.04.042
8. Teimouri, R. (2019). Optimization of residual stress field in ultrasonic assisted burnishing process. *International Journal of Lightweight Materials and Manufacture*, Vol. 2(4), pp. 346–354. https://doi.org/10.1016/j.ijlmm.2019.04.009
9. Caudill, J., Schoop, J., Jawahir, I. S. (2019). Correlation of surface integrity with processing parameters and advanced interface cooling/lubrication in burnishing of Ti-6Al-4V alloy. *Adv. Mater. Process. Technol*, Vol. 5(1), pp. 53–66. https://doi.org/10.1080/2374068X.2018.1511215
10. Caudill, J., Schoop, J., Jawahir, I. S. (2019). Producing sustainable nanostructures in Ti-6Al-4V alloys for improved surface integrity and increased functional life in aerospace applications by cryogenic burnishing. *Procedia CIRP*, Vol. 80, pp. 120–125. https://doi.org/10.1016/j.procir.2018.12.022
11. Huang, B., Kaynak, Y., Sun, Y., Khraisheh, M. K., Jawahir, I. S. (2022). Surface layer modification by cryogenic burnishing of Al 7050-T7451 alloy with near ultra-fine grained structure. *Journal of Manufacturing Science and Engineering*, Vol. 144(3). https://doi.org/10.1115/1.4051786
12. Travieso-Rodríguez, J. A., Jerez-Mesa, R., Gómez-Gras, G., Llumà-Fuentes, J., Casadesús-Farràs, O., Madueño-Guerrero, M. (2019). Hardening effect and fatigue behavior enhancement through ball burnishing on AISI 1038. *Journal of Materials Research and Technology*, Vol. 8(6), pp. 5639–5646. https://doi.org/10.1016/j.jmrt.2019.09.032
13. Pu, Z., Song, G.-L., Yang, S., Outeiro, J. C., Dillon Jr., O. W., Puleo, D. A., Jawahir, I. S. (2012). Grain refined and basal textured surface produced by burnishing for improved corrosion performance of AZ31B Mg alloy. *Corrosion Science*, Vol. 57, pp. 192–201. https://doi.org/10.1016/j.corsci.2011.12.018
14. Yang, S., Umbrello, D., Dillon, O. W., Puleo, D. A., Jawahir, I. S. (2015). Cryogenic cooling effect on surface and subsurface microstructural modifications in burnishing of Co–Cr–Mo biomaterial. *Journal of Materials Processing Technology*, Vol. 217, pp. 211–221. https://doi.org/10.1016/j.jmatprotec.2014.11.004
15. Livatyali, H., Has, E., Türköz, M. (2020). Prediction of residual stresses in ball burnishing Ti_6Al_4V thin sheets. *The International Journal of Advanced Manufacturing Technology*, Vol. 110(3–4), pp. 1083–1093. https://doi.org/10.1007/s00170-020-05837-2
16. Chomienne, V., Valiorgue, F., Rech, J., Verdu, C. (2016). Influence of ball burnishing on residual stress profile of a 15-5PH stainless steel. *CIRP Journal of Manufacturing Science and Technology*, Vol. 13, pp. 90–96. https://doi.org/10.1016/j.cirpj.2015.12.003
17. Yu, H., Yan, M., Li, J., Godbole, A., Lu, C, Tieu, K., Li, H., Kong, C. (2018). Mechanical properties and microstructure of a Ti-6Al-4V alloy subjected to cold rolling, asymmetric rolling and asymmetric cryorolling. *Materials Science and Engineering: A*, Vol. 710, pp. 10–16. https://doi.org/10.1016/j.msea.2017.10.075
18. Yang, S., Umbrello, D., Dillon, O. W., Jawahir, I. S. (2022). Numerical investigation of dynamic recrystallization induced microstructural evolution in cryogenic burnishing of Co-Cr-Mo biomaterial. *Journal of Materials Engineering and Performance*, Vol. 31(8), pp. 6904–6921. https://doi.org/10.1007/s11665-022-06738-z
19. Zhang, T., Bugtai, N., Marinescu, I. D. (2015). Burnishing of aerospace alloy: A theoretical–experimental approach. *Journal of Manufacturing Systems*, Vol. 37, pp. 472–478. https://doi.org/10.1016/j.jmsy.2014.11.004
20. Swirad, S., Wdowik, R. (2019). Determining the effect of ball burnishing parameters on surface roughness using the Taguchi method. *Procedia Manufacturing*, Vol. 34, pp. 287–292. https://doi.org/10.1016/j.promfg.2019.06.152
21. Lu, H., Wu, L., Wei, H., Cai, J., Luo, K., Xu, X., Lu, J. (2022). Microstructural evolution and tensile property enhancement of remanufactured Ti_6Al_4V using hybrid manufacturing of laser directed energy deposition with laser shock peening. *Additive Manufacturing*, Vol. 55, 102877. https://doi.org/10.1016/j.addma.2022.102877